Journal of Advanced Marine Engineering and Technology, Vol. 49, No. 6, pp. 590~601, 2025
J. Advanced Marine Engineering and Technology (JAMET)
https://doi.org/10.5916/jamet.2025.49.6.591

ISSN 2234-7925 (Print)
ISSN 2765-4796 (Online)
Original Paper

Comparison of dynamic structural responses of blast walls subjected to hydrogen blast loads

Hyun-Ho Lee[1] · Dong-Kyeong Yang[2] · Jung-Kwan Seo[†]

(Received August 14, 2025 ; Revised September 24, 2025 ; Accepted November 27, 2025)

Abstract: Shipbuilding and maritime industries are increasingly focusing on alternative fuels to achieve decarbonization. Among the various options, hydrogen fuel is regarded as the most promising; however, it features an inherent and significant explosion risk. To address this risk, hydrogen blast load scenarios were selected and applied to blast walls typically installed in offshore structures. The dynamic structural responses of these blast walls were analyzed and compared in terms of the maximum displacement, fracture occurrence, and stress and plastic strain distributions using both single-degree-of-freedom and finite element methods. Lastly, a conceptual blast wall design was proposed, and its applicability to blast wall design was evaluated.

Keywords: Dynamic structural response, Blast walls, Hydrogen blast load, Finite element method, Single-degree-of-freedom method

1. Introduction

In accordance with the IMO's decarbonization strategy, shipbuilding and maritime industries are increasingly focusing on alternative fuels to replace conventional fossil fuels. Among various alternative fuels, hydrogen is considered one of the most promising owing to its zero greenhouse gas emissions during use. Accordingly, extensive research has been conducted from multiple perspectives regarding the practical applications and commercialization of hydrogen fuel.

However, the use of hydrogen introduces new safety challenges, in particular leakage and explosion risks. Hydrogen possesses a low boiling point and Minimum Ignition Energy (MIE), along with wide flammability limits **[1]**, which makes it more explosive than other alternative fuels. Additionally, its higher combustion rate and flame propagation speed contribute to more severe blast loads compared with conventional hydrocarbon fuels **[2][3]**.

Figure 1 shows post-accident photographs of hydrogen explosion accidents that occurred in the Republic of Korea and Norway in 2019, which demonstrate the risk of hydrogen explosions **[4][5]**. Although the accident scenes were equipped with explosion-proof systems in accordance with relevant regulations and the amount of hydrogen involved was relatively small, the accidents resulted in significant casualties and property damage. Following these accidents, regulations related to hydrogen leakage and explosions have been strengthened, and subsequent research has intensified.

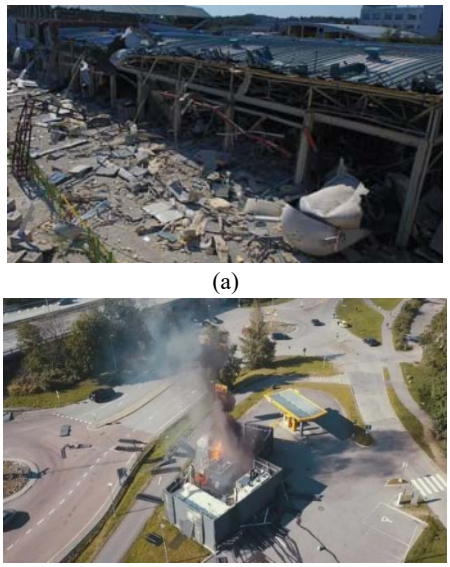

(a)

(b)

Figure 1: Photographs of hydrogen explosion accidents in (a) the Republic of Korea and (b) Norway

† Corresponding Author (ORCID: https://orcid.org/0000-0002-3721-2432): Professor, Department of Naval Architecture and Ocean Engineering & The Korea Ship and Offshore Research Institute, Pusan National University, 2, Busandaehak-ro 63beon-gil, Geumjeong-gu, Busan, 46241, Republic of Korea, E-mail: seojk@pusan.ac.kr, Tel: 051-510-2415

1 Ph. D. Student, Department of Naval Architecture and Ocean Engineering, Pusan National University, E-mail: leehono@pusan.ac.kr

2 M. S. Student, Department of Naval Architecture and Ocean Engineering, Pusan National University, E-mail: dongkyeong@pusan.ac.kr

Studies analyzing the dynamic response of structures subjected to hydrogen blast loads can serve as valuable references for the safety design of facilities with a high risk of hydrogen explosion. Mo *et al.* **[6]** predicted the structural response of a spherical tank exposed to hydrogen-blended natural gas explosions using TNT-equivalent and Arbitrary Lagrangian-Eulerian (ALE) methods, and examined the effects of the hydrogen-blend ratio, pillar thickness, and standoff distance. Wang *et al.* **[7]** experimentally observed the effect of volumetric blockage ratio on hydrogen explosion loads and the resulting structural responses, and identified the correlation between the blockage ratio and structural responses. Hao *et al.* **[8]** conducted 48 vented explosion experiments on a 40-foot container and investigated the effects of vent location, obstacle configuration, ignition position, and hydrogen concentration on its structural behavior. Du *et al.* **[9]** numerically analyzed mode I crack propagation of a tube under internal hydrogen static and detonation loadings, with emphasis on crack dynamics, energy absorption and other characteristics. Russo *et al.* **[10]** conducted a probabilistic risk assessment on high-pressure hydrogen pipelines to estimate the potential harm to humans and buildings exposed to pipeline explosions, and proposed a safe separation distance. In addition to these studies, a wide range of studies have provided important findings regarding the dynamic responses of structures under hydrogen blast loads **[11]-[20]**. However, because most of the structures analyzed for their dynamic structural responses feature simple and fundamental structural forms, such as square panels, storage tanks, and containers, directly applying these findings to structural design is challenging. In particular, studies investigating the dynamic responses of structures commonly used in ships and offshore structures are extremely rare.

In this study, blast load scenarios that reflect hydrogen explosion characteristics were applied to blast walls typically used in offshore structures. The dynamic structural responses of these blast walls were analyzed and compared in terms of key design parameters, such as maximum displacement and fracture occurrence. A simplified analysis method based on degree-of-freedom reduction and numerical simulation using the Finite Element Method (FEM) were employed to analyze the dynamic structural response. Lastly, a hybrid blast wall combining the advantages of existing blast wall designs was proposed, and its applicability was evaluated by analyzing its structural response under hydrogen blast load scenarios.

2. Modeling Methods for Dynamic Structural Response Analysis of Blast Walls

Stiffened and corrugated blast walls, which are typically installed on offshore structures, were selected as target structures. Although blast walls generally feature site-specific designs based on their installation locations, the designs and dimensions of the target structures in this study were determined based on related studies and design guidance **[21][22]**.

The dynamic structural responses of the target structures were analyzed using two approaches. The first approach is an analytical approach based on the Single-Degree-of-Freedom (SDOF) method. The SDOF method simplifies the dynamic behavior of a structure by modeling it as an SDOF system. Although this method provides limited accuracy and detail in describing the dynamic behavior compared with the FEM, it offers advantages in terms of computational efficiency and modeling ease. In particular, the Pressure-Impulse (P-I) diagram, which is a preliminary design tool, was primarily developed based on the SDOF method. Additionally, this method was introduced as a structural analysis method in the recommended practice published by a classification society **[23]**. In this study, the Biggs method **[24]**—one of the simplest and most practical SDOF methods—was used to analyze dynamic structural responses. It is based on the following equation:

$$\overline{m}\ddot{w} + \overline{k}w = \overline{F}(t) \tag{1}$$

where, $\overline{m}$ is the generalized mass, $\overline{k}$ is the generalized elastic bending stiffness, $\overline{F}(t)$ is the generalized force and w is the displacement.

In deriving the generalized coefficients in **Equation (1)**, the analysis scope was limited to a stiffened or corrugated panel, which is a structural member directly subjected to blast loads, and supporting structures were excluded. Since the Biggs method does not account for material plasticity, a linear elastic material model was used in simulations, with a density of 7.85 t/mm³ and an elastic modulus of 200,000 MPa. Simply-supported boundary conditions were applied for conservative analyses.

The second approach is numerical simulation using the FEM. As a type of Multi-Degree-of-Freedom (MDOF) method, it is frequently adopted as an analytical approach in structural design. However, because both the preprocessing and solving stages are relatively time consuming, this approach could have a limitation

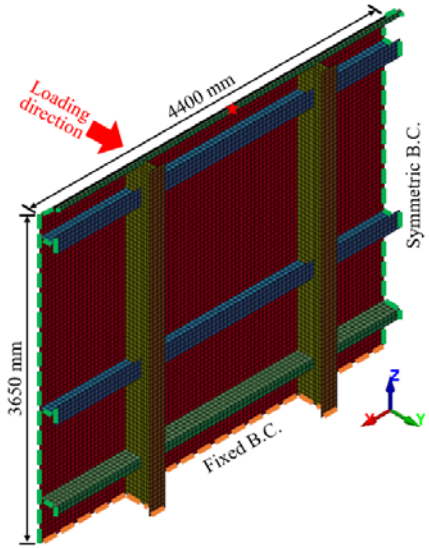

Figure 2: Numerical model of stiffened blast wall

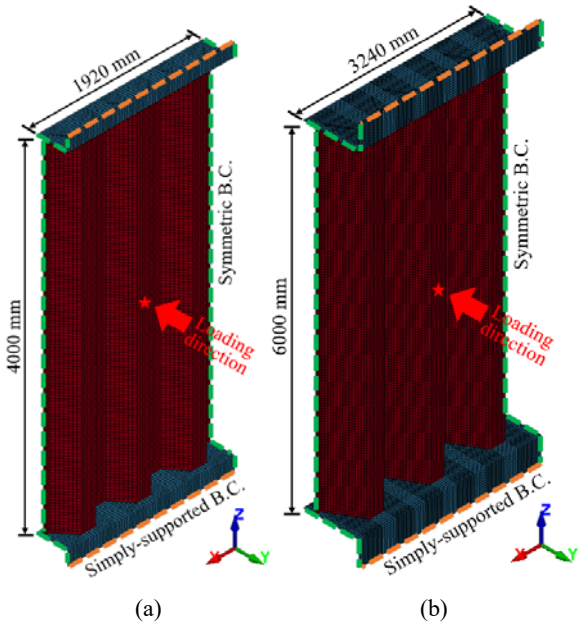

Figure 3: Numerical models of corrugated blast walls with (a) intermediate and (b) deep sections

in terms of its application to parametric studies. Moreover, the prediction accuracy would be significantly reduced if the user lacks sufficient knowledge and experience during the preprocessing stage.

The numerical model used in this study was developed based on a validated model developed by Lee and Seo **[25]**, whose accuracy was confirmed through comparison with experimental results. **Figure 2** shows the numerical model of a stiffened blast wall with applied boundary conditions and loading directions. The blast wall has a geometric configuration with one side fixed to the structure's deck, while the opposite side is open **[21]**. It comprises a panel that directly receives blast loads and multiple stiffeners, which contribute to most of the bending rigidity. All the structural members were assumed to be made of AH36 high-tensile steel.

Figure 3 illustrates the numerical model of a corrugated blast wall. Two types of corrugated blast walls corresponding to the intermediate and deep sections presented in the design guidance were modeled **[22]**. The corrugated blast walls were not directly connected to the structure's deck by its corrugated panel but rather through angle-type supports attached to both sides of the panel, which were connected to stiffer structural members. The analysis scope covered a corrugated panel and the first supports attached to it. Unlike the stiffened blast wall, whose boundary conditions were predetermined in a previous study, simply supported boundary conditions were applied in the numerical model to provide a conservative prediction of the structural response of the corrugated blast walls. Both the panel and supports were assumed to be made of duplex stainless steel 2205.

Table 1: Comparison of mass and natural period for different blast walls

Type	Numerical model	Mass (t)	Natural period, T_N (s)
Stiffened blast wall	**Figure 2**	2.39	0.054
Corrugated blast wall with intermediate section	**Figure 3(a)**	1.37	0.024
Corrugated blast wall with deep section	**Figure 3(b)**	5.06	0.047

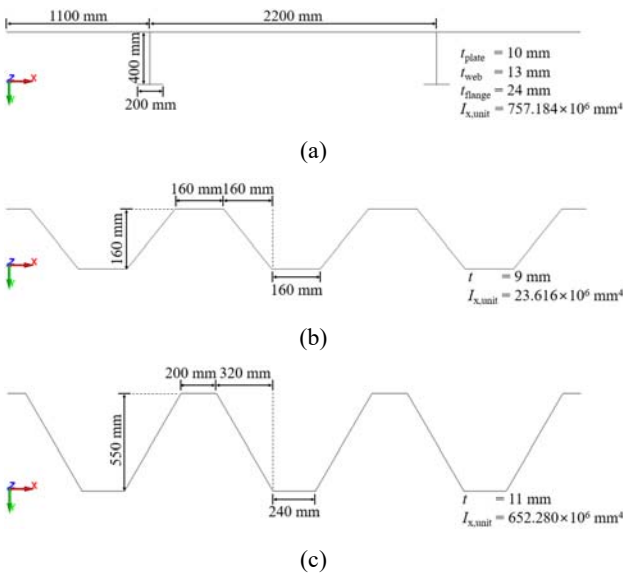

Figure 4: Comparison of cross-sectional configurations of blast wall types: (a) stiffened blast wall, (b) corrugated blast wall with intermediate section, and (c) corrugated blast wall with deep section

Table 1 shows a comparison of the mass and natural period (T_N) associated with the primary mode shape for each blast wall type. Each blast wall exhibited distinct mass and the natural period. **Figure 4** shows a comparison of the cross-sectional configurations of each blast wall type and the corresponding x-direction moments of inertia for their repeating segments, with the scale differing from the actual geometry. Among the three blast wall types, the stiffened blast wall exhibited the highest moment of inertia. Furthermore, compared with the corrugated blast walls, it exhibited a considerably higher moment of inertia relative to its mass.

All the numerical models adopted a bilinear elasto–plastic material model, and nominal values of the material properties were used to ensure both generality and conservatism in the simulation results. The nominal material properties of these models are listed in **Table 2**. The blast loads are characterized by short rising time and duration, which result in high strain rates during deformation. To account for the strain rate effect on the structural response, the following Cowper–Symonds equation was applied **[26]**:

$$\sigma_{Yd}/\sigma_Y = 1.0 + (\dot{\varepsilon}/C)^{1/q} \quad (2)$$

where, σ_{Yd} and σ_Y are the dynamic and static yield strengths, respectively, $\dot{\varepsilon}$ is the strain rate, and C and q are the strain rate parameters. The strain rate parameters for each material were determined with reference to relevant literature **[27]**, and were listed in **Table 2**.

A four-node fully integrated shell element was adopted as the element type, and the element size was determined to be within the range of 30–40 mm based on the convergence study results of related studies **[25][28]**. Blast loads were applied to the entire surface of the blast walls in the form of time-varying pressure in the direction indicated by the red arrows in **Figures 2** and **3**.

Table 2: Nominal material properties used in numerical model

Material properties	AH36 high-tensile steel	Duplex SS2205
Density	7.85×10^{-9} t/mm^3	
Elastic modulus	200,000 MPa	
Poisson's ratio	0.3	
Yield strength	355 MPa	450 MPa
Tangent modulus	0.3% of elastic modulus	
Static fracture strain	0.25	0.30
Cowper-Symonds constants	C of 3200.0 / q of 5.0	C of 100.0 / q of 4.0

These time-varying blast loads corresponded to the blast load scenarios discussed in the following section. To account for the damping effect in the structural response, a damping coefficient of $0.4\pi/T_N$ was applied to all directional damping forces. This coefficient, which is recommended in the LS-DYNA manual **[29]**, corresponds to 10% of the critical damping and represents an empirical and practical value commonly used in numerical simulations of dynamic structural responses. An explicit solver in LS-DYNA was used in the simulations **[29]**.

Contact interactions were defined as surface-to-surface interactions between the corrugated panel and angle-type support, and a single-surface contact was applied to the corrugated panel itself. The characteristic length for the time step calculation was defined as the element area divided by the maximum element edge length, and the simulation termination times were set to three times the blast load duration to fully capture the structural responses, including inertial effects.

Although the validation of the numerical model was not repeated in this study, the simulation results can be considered as suitable for providing reliable predictions of the dynamic structural response of the blast wall. This assessment is supported by previous work, including that of Lee and Seo **[25]**, which demonstrated the accuracy of an identical modeling approach for a corrugated blast wall.

3. Dynamic Structural Response of Blast Walls Subjected to Hydrogen Blast Loads

Hydrogen has a significantly faster combustion rate and flame propagation speed compared with hydrocarbons, thus resulting in distinct differences in the blast load characteristics. In this study, hydrogen blast load scenarios were selected separately from conventional hydrocarbon-based scenarios to account for these differences. The selected scenarios were based on the characteristics of hydrogen blast loads analyzed by Lee and Seo **[25]**. **Table 3** presents 90 hydrogen blast load scenarios. All the scenarios were modeled as triangular impulse loads, and their negative phase was not considered. **Figure 5** shows an example of an actual blast load and its idealized triangular impulse load profile, which was defined by the peak overpressure (p_{peak}), rising time (t_r), and duration (t_d). The upper limit of the peak overpressure in the scenarios was set to 1.2 MPa. This was based on the nominal hydrocarbon peak overpressure of 0.3 MPa and the observation that the hydrogen peak overpressure was approximately four times greater. For the duration, the lower limit was set to 0.01 s

Table 3: Hydrogen blast load scenarios

Scenario no.	Peak overpressure (p_{peak}, MPa)	Duration (t_d, s)	Rising time (t_r, s)
1	0.05	0.01	0.0075 (75% of t_d)
2		0.02	0.015 (75% of t_d)
3		0.03	0.0225 (75% of t_d)
4		0.04	0.03 (75% of t_d)
5		0.06	0.045 (75% of t_d)
6		0.08	0.06 (75% of t_d)
7		0.10	0.075 (75% of t_d)
8		0.13	0.0975 (75% of t_d)
9		0.16	0.12 (75% of t_d)
10		0.20	0.15 (75% of t_d)
11-20	0.1	0.01-0.20	75% of t_d
21-30	0.15	0.01-0.20	75% of t_d
31-40	0.2	0.01-0.20	50% of t_d
41-50	0.4	0.01-0.20	25% of t_d
51-60	0.6	0.01-0.20	0% of t_d (No t_r)
61-70	0.8	0.01-0.20	0% of t_d (No t_r)
71-80	1.0	0.01-0.20	0% of t_d (No t_r)
81-90	1.2	0.01-0.20	0% of t_d (No t_r)

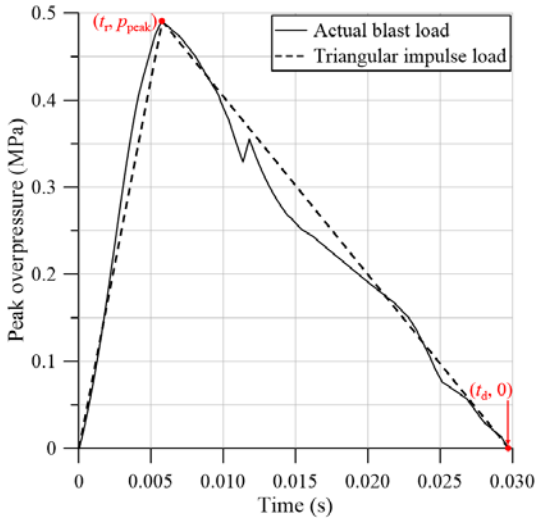

Figure 5: Example of actual and idealized triangular blast load profiles

to ensure that the blast load scenarios were realistic and within the impulsive domain **[30]**. The upper limit was set to 0.2 s, which was sufficiently long that dynamic structural response due to inertia was hardly observed. For gas explosions, it is generally understood that the peak overpressure and duration are inversely related. However, Lee and Seo **[25]** observed that a wide range of durations may occur, even for the same peak overpressure, depending on the explosion conditions. Therefore, scenarios were constructed to include all possible combinations of peak overpressure and duration. As the peak overpressure increased, triangular impulse loads with smaller rising time-to-duration ratios

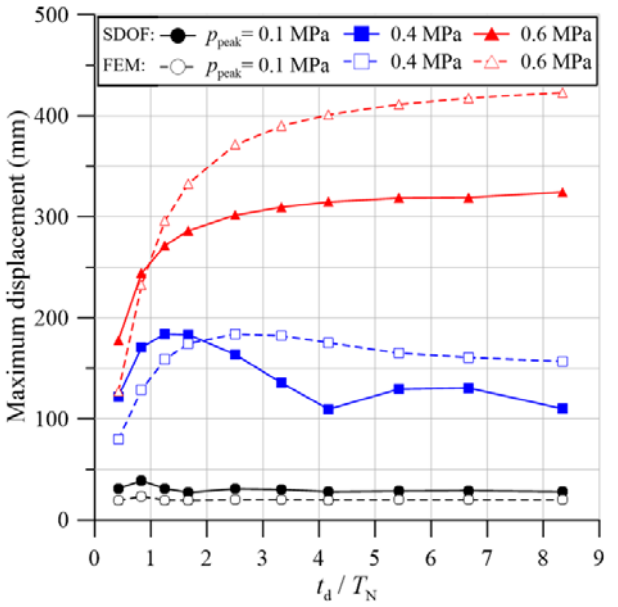

Figure 6: Comparison of maximum displacements predicted using SDOF and FE methods

were applied. This is because an inverse relationship between the peak overpressure and rising time-to-duration ratio was observed.

The analytical approach was first employed to analyze the dynamic structural response of the blast wall. To validate this approach, the predicted results were compared with those obtained from numerical simulations. Both approaches were applied to the corrugated blast wall with an intermediate section, and the y-direction displacements at the center of the wall were compared. **Figure 6** shows a comparison of the maximum y-direction displacements for the blast load scenarios corresponding to peak overpressures of 0.1 MPa (Scenarios 11–20), 0.4 MPa (Scenarios 41–50), and 0.6 MPa (Scenarios 51–60). The scenarios were distinguished in the legend and along the x-axis, where the durations were non-dimensionalized by the natural period (T_N) values listed in **Table 1**.

For the blast load scenarios with a peak overpressure of 0.1 MPa, both the analytical and numerical approaches predicted that the maximum structural responses would occur at t_d/T_N values of 0.5–1.0. This is because the blast wall predominantly experienced elastic deformation, and the structural response was amplified owing to the resonance between the duration and the natural period. However, because the SDOF method adopted in this study did not account for damping effects and excluded the supports in the analysis scope, the analytical approach overestimated the maximum displacements compared with the numerical simulations. In the load scenarios with peak overpressures of 0.4 and

0.6 MPa, local plastic deformation occurred within the blast wall, and the maximum displacements increased significantly. However, the SDOF method underestimated the maximum displacements with a relative error of up to approximately 40% because it assumed that the target structure remained elastic. Hydrogen explosions generally have higher peak overpressures than hydrocarbon explosions and are more likely to cause plastic deformation in blast walls. The previous comparison indicates that the SDOF method may not provide reliable predictions of the structural response of blast walls subjected to hydrogen blast loads because of several inherent modeling limitations.

Unlike previous studies on hydrocarbon blast loads with relatively low peak overpressures, this study considered hydrogen blast loads, which are more likely to induce plastic deformation in blast walls. The results presented in **Figure 6** highlight the limited applicability of the conventional SDOF method under such conditions. Therefore, in the subsequent analysis, only FEM-based numerical simulations were employed to investigate the dynamic structural response of blast walls.

Figures 7(a), **(b)** and **(c)** present the maximum y-direction displacements for each blast wall type under the hydrogen blast load scenarios. The displacements were measured at the locations where the maximum deformation occurred in the blast walls, as indicated by the red stars in **Figures 2** and **3**. The maximum displacement in the direction parallel to the blast load propagation is an important structural response parameter that serves as a quantitative criterion for blast wall design. Accordingly, **Figure 7** shows the recommended deflection limits proposed by FABIG **[31]**, i.e., span/40 and span/25, as shown by the dashed and dash-dotted red lines, respectively. These limits, which provide widely accepted design recommendations for offshore blast walls and are typically referenced in regulatory and industrial design guidelines, were used to evaluate the acceptability of the blast wall deformation. Moreover, for blast walls subjected to blast loads, if even a minor localized fracture occurs, the walls may be regarded as having reached the Ultimate Limit State (ULS), where they no longer fulfill their structural function. Such cases were excluded from **Figure 7**; therefore, the discontinuity in the curve indicates that fracture occurred in the corresponding load scenario.

The maximum displacement increased for all the blast walls as the peak overpressures increased. However, an increase in duration did not necessarily lead to a corresponding increase the maximum displacement. For blast load scenarios with a relatively low peak overpressure, elastic deformation occurred

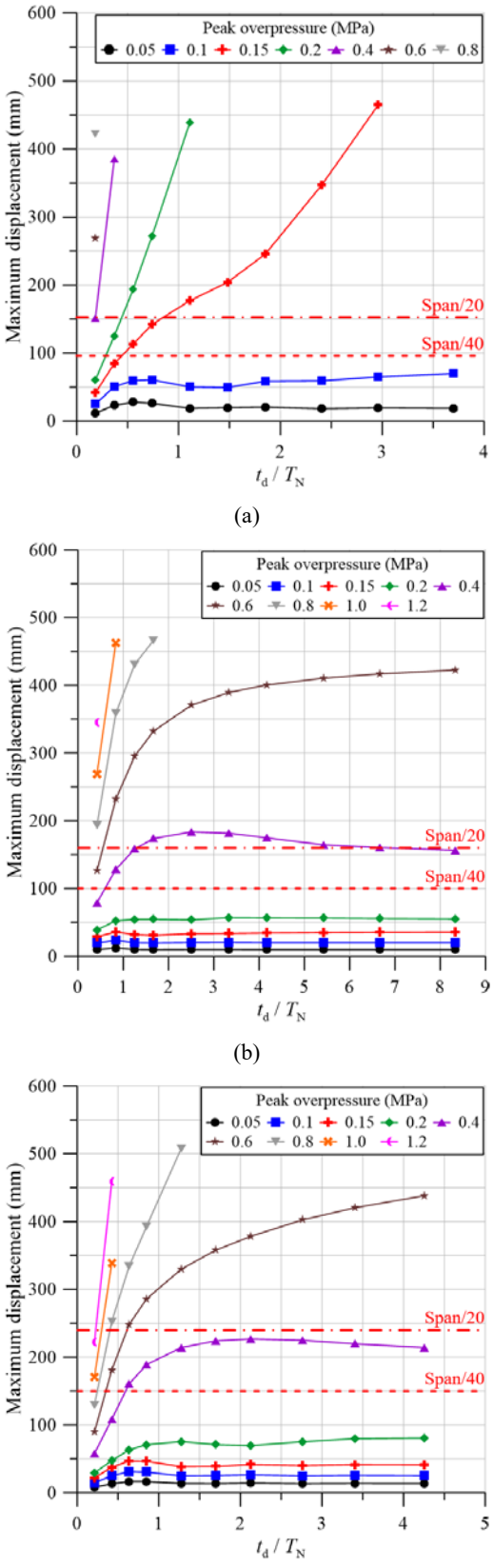

Figure 7: Maximum displacements of (a) stiffened blast wall and corrugated blast walls with (b) intermediate and (c) deep sections, corresponding to hydrogen blast load scenarios

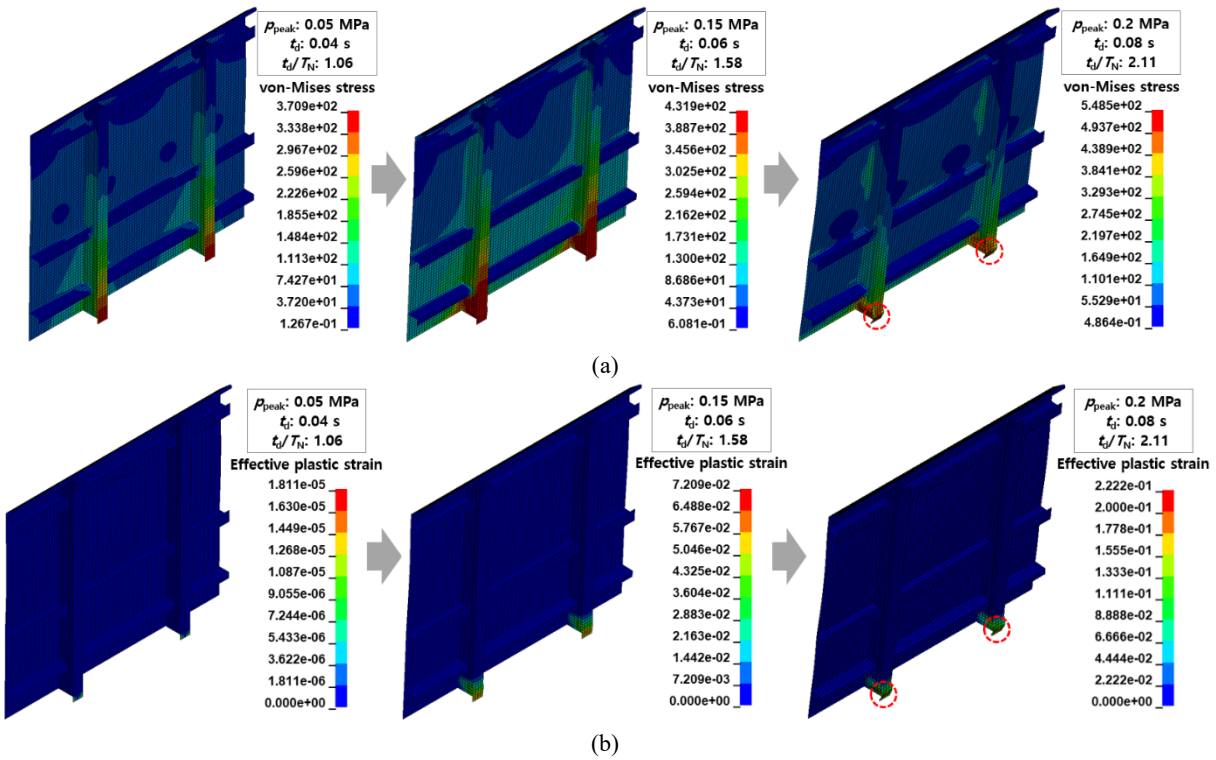

Figure 8: (a) Von-Mises stress and (b) effective plastic strain distributions of stiffened blast wall under representative hydrogen blast load scenarios

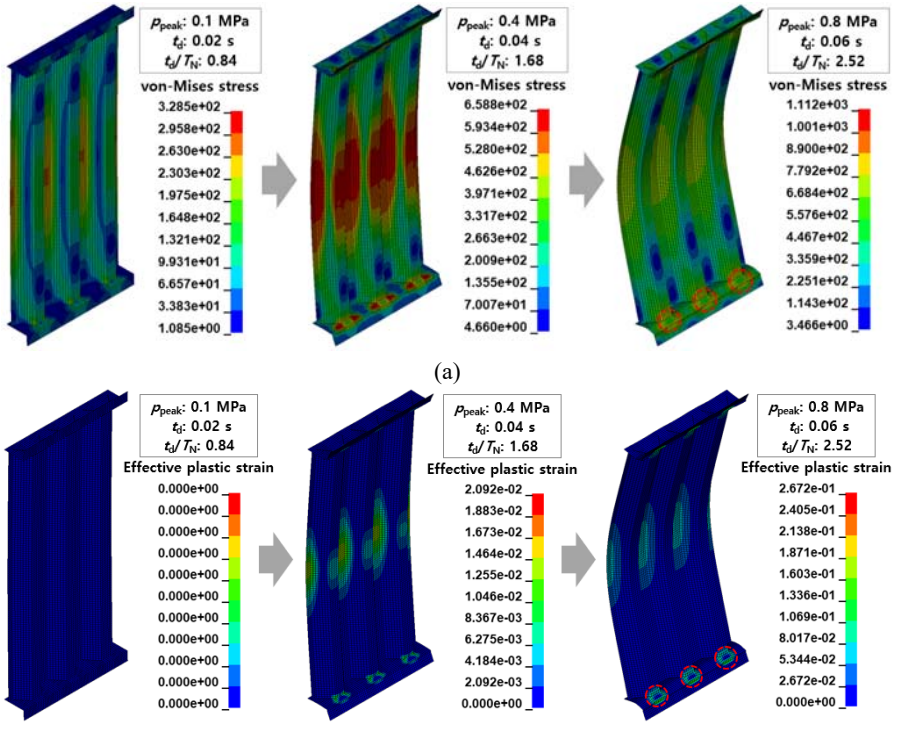

Figure 9: (a) Von-Mises stress and (b) effective plastic strain distributions of corrugated blast wall under representative hydrogen blast load scenarios

predominantly, thus making the effect of resonance on the structural response more significant. Consequently, the maximum structural response was observed when t_d/T_N was approximately 0.5. If the blast wall were to deform perfectly in its primary mode, then the resonance effect would cause the maximum response to occur near at $t_d/T_N \approx 0.5$. However, although deformation was

primarily reflected the primary mode, several minor modes were superimposed, thus causing the maximum response to occur under t_d/T_N values of 0.5–1.0 for all blast wall types.

As the peak overpressure increased, the blast load duration at which the maximum structural response occurred increased as well. This is attributed to the occurrence of plastic deformation in the blast walls, which reduced the structural stiffness, thereby increasing the natural period **[32][33]**. In the blast load scenarios with a peak overpressure of 0.6 MPa or higher, right-angled triangular blast loads without rising times were applied. In these cases, the effects of stiffness reduction and blast load shape on the structural response were maximized. Therefore, the maximum displacement increased nonlinearly with increasing blast load duration.

The blast load scenarios at which the recommended deflection limits were reached or fracture began to occur varied among the different blast wall types. The stiffened blast wall reached the deflection limits and fracture at peak overpressures that were 0.25 and 0.65 MPa lower than those for the corrugated blast walls, respectively. Although the blast wall types exhibited different stiffnesses and strengths, the design criteria were not satisfied and the ULS was reached prior to applying all hydrogen blast load scenarios. This indicates that blast walls designed for hydrocarbon blast loads might have insufficient structural capacity to withstand hydrogen blast loads, which tend to exhibit higher peak overpressures than those of hydrocarbons.

Even under the same blast load scenario, the stiffened blast wall exhibited a larger displacement than the corrugated blast walls. This difference is attributed to the boundary conditions of the blast walls and the differences in the directions of stresses developed during deformation. As shown in **Figure 2**, the stiffened blast wall was installed with one end fixed, which caused a larger deformation compared with the case where both ends were fixed **[34]**. Additionally, the panel of the stiffened blast wall was directly attached to the deck, thus causing a significant stress concentration at the fixed end. This may result in a more rapid localized plastic deformation than that in the corrugated blast walls. These differences were confirmed by comparing the deformation shapes and structural responses of the stiffened blast wall and the corrugated blast wall with the intermediate section, as shown in **Figures 8** and **9**.

Figures 8 and **9** sequentially present the von-Mises stress and effective plastic strain distributions for representative blast load scenarios: scenarios in which the blast walls primarily experienced elastic deformation and the maximum structural responses occurred when the blast load duration was approximately 0.5 times the wall's natural period (first column of **Figures 8** and **9**); the first scenario in which the maximum displacements exceeded span/20 (second column); and the first scenario in which fracture was observed (third column). For the first and second columns, the distributions are shown at the time of maximum deformation, whereas for the third column, they are shown immediately before fracture occurs. The locations of the initial fractures are indicated by dashed red circles in the figures.

The stiffened blast wall shown in **Figure 8** was designed such that it deformed and tilted in the direction of the stiffeners when subjected to blast loads. This deformation mode did not pose a significant issue when the blast load had a relatively low peak overpressure, which primarily resulted in elastic deformation. However, in the load scenario corresponding to the second column, if the blast load induced sufficiently large compressive stresses that cause buckling at the stiffener ends, then the stiffness of the stiffener would decrease rapidly after buckling. As stiffeners contribute primarily to the blast resistance of the wall, buckling in these members causes deformation to increase nonlinearly. Shortly thereafter, similar to the load scenario corresponding to the third column, fractures occurred near the buckling locations. In the panel that directly received blast loads, relatively small stresses and plastic strains were observed compared with those in the stiffeners, even immediately before fracture. This demonstrates that, in the stiffened blast wall, the panel may not fully function as the primary blast-resisting member due to the geometric configuration of the blast wall.

Unlike the stiffened blast wall, the corrugated blast wall exhibited stress distributions across the entire structure, thus indicating that both the corrugated panel and supports deformed simultaneously to absorb the blast loads. Owing to the presence of sharp corners at the panel–support joints, which induce local stress concentration, significant stress and plastic strain were observed at these locations, eventually leading to fracture, as illustrated in the load scenario corresponding to the third column of **Figure 9**. Nevertheless, the analysis of the unfolding deformation shapes confirmed that tensile stress occurred predominantly at these joints, thus resulting in a lower risk of local buckling compared with the stiffened blast wall. Therefore, special attention should be paid not only to the design of the panel, which is the primary structural member subjected to blast loads, but also to the design of the panel-support connections to prevent

premature structural collapse of the blast walls. The von-Mises stress and effective plastic strain distributions for the corrugated blast wall with a deep section are not presented because they exhibited similar trends in structural responses to those shown in **Figure 9**. This is because, although the moment of inertia was increased by the deeper section, the blast wall span was increased as well, thereby increasing the moment arm.

Most blast walls installed on offshore structures exhibit the configurations shown in **Figures 2** and **3**. In this study, a hypothetical hybrid blast wall that combined the bending-strength advantage of a stiffened panel and the geometric advantage of an angle-type support was numerically modeled, as illustrated in **Figure 10(a)**. Except for the cross-sectional shape of the stiffened panel, all other design parameters, including the material properties, mass, overall span, and support dimensions, were set identical to those of the corrugated blast wall with an intermediate section. The cross-sectional shape was determined by placing stiffeners at the corrugated panel corrugations while maintaining the same cross-sectional area as that of the corrugated panel, as shown in **Figure 10(b)**. The dynamic structural response of the hybrid blast wall was investigated under hydrogen blast load scenarios to examine its applicability to blast wall design.

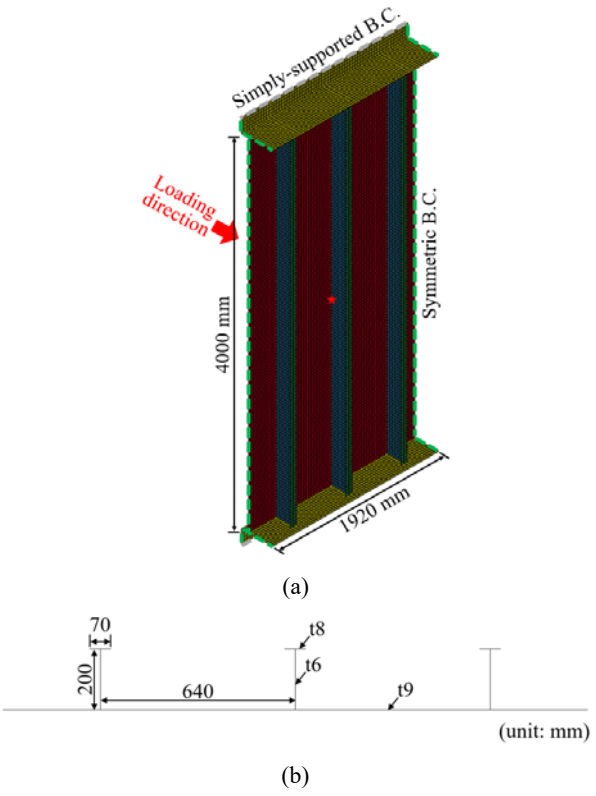

Figure 10: (a) Numerical model and (b) cross-section configuration of hybrid blast wall

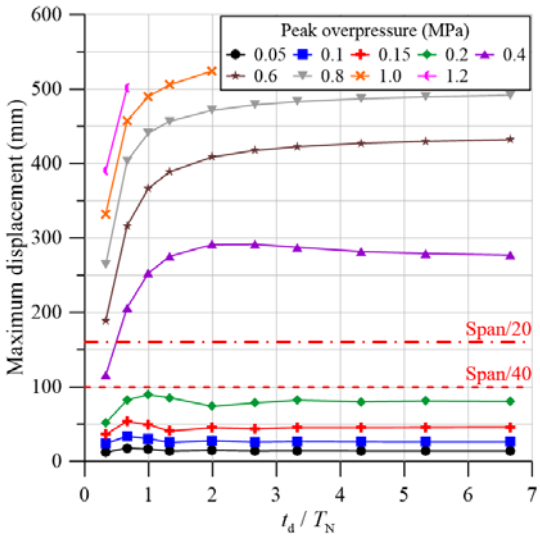

Figure 11: Maximum displacements of hybrid blast wall corresponding to hydrogen blast load scenarios

Figure 11 presents the maximum y-direction displacements of the hybrid blast wall under the hydrogen blast load scenarios. In the load scenarios with relatively low peak overpressures (not exceeding 0.4 MPa), the hybrid blast wall exhibited greater displacement than the corrugated blast wall with an intermediate section. This difference is attributed to the sequence of yielding-induced large deformation. Whereas the corrugated blast wall yielded first in the relatively short supports followed by the panel as the peak overpressure increased, the hybrid blast wall experienced large deformation caused by yielding in the relatively long panel prior to yielding in the supports. From the load scenarios with a peak overpressure of 0.6 MPa, since the yielding-induced large deformation occurred in the panel of the corrugated blast wall as well, comparable maximum displacements between the hybrid and corrugated blast walls were observed. Moreover, compared with the case of the corrugated blast wall, the number of load scenarios without an observed fracture increased, and the peak overpressure at which fracture first occurred was 0.2 MPa higher. These increases show that the integration of a stiffened panel with angle-type supports can effectively delay fractures in blast walls.

Figures 12(a) and **(b)** show the von-Mises stress and effective plastic strain distributions of the hybrid blast wall, respectively, along with their deformation shapes. These are presented using the same methodology as that in **Figures 8** and **9**. As the peak overpressure of the blast load increased, yielding occurred progressively in the flange, the web, and the joints between the panel and supports. This progression differs from the deformation

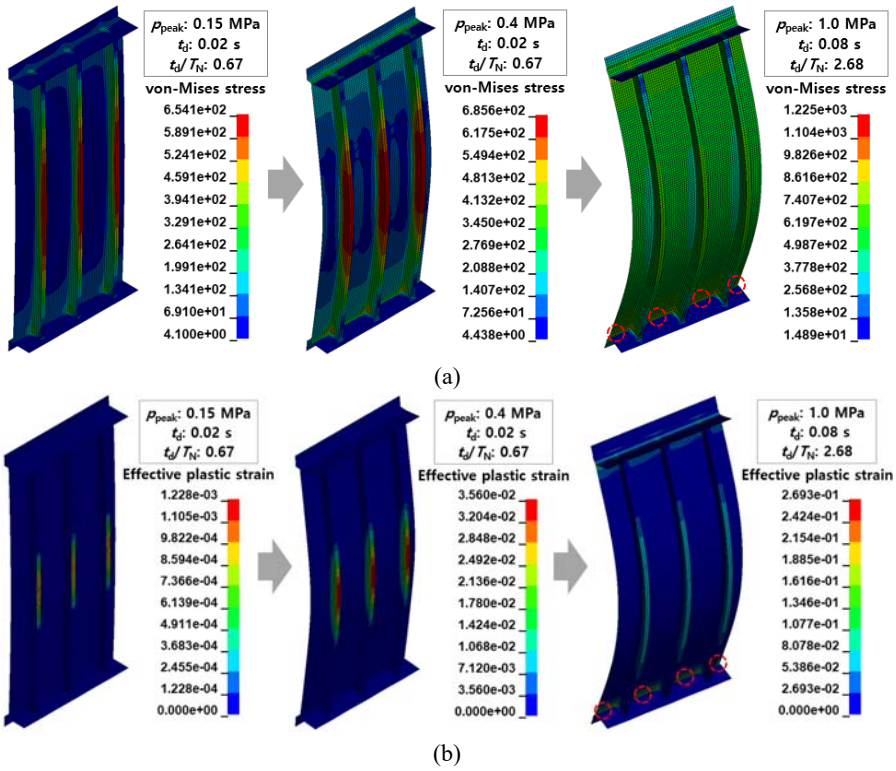

Figure 12: (a) Von-Mises stress and (b) effective plastic strain distributions of hybrid blast wall under representative hydrogen blast load scenarios

Table 4: Comparison of blast load scenarios corresponding to first yielding and first fracture for each blast wall type

Type	Blast load at first yielding	Blast load at fracture initiation
Hybrid blast wall	p_{peak} = 0.1 MPa, t_d = 0.01 s	p_{peak} = 1.0 MPa, t_d = 0.08 s
Stiffened blast wall	p_{peak} = 0.05 MPa, t_d = 0.03 s	p_{peak} = 0.15 MPa, t_d = 0.20 s
Corrugated blast wall with intermediate section	p_{peak} = 0.15 MPa, t_d = 0.01 s	p_{peak} = 0.8 MPa, t_d = 0.06 s
Corrugated blast wall with deep section	p_{peak} = 0.1 MPa, t_d = 0.03 s	p_{peak} = 0.8 MPa, t_d = 0.08 s

modes of corrugated blast walls proposed by Lee and Seo **[25]** and supports a previous description of the sequence of yielding-induced large deformations. Fracture initially occurred at the joints, particularly in the areas without stiffeners. Therefore, the hybrid blast wall offers an easier reinforcement method of adding stiffeners than corrugated blast walls. Although this method can slightly increase the mass of the blast wall, the displacement under the same blast load would decrease and the occurrence of fractures would be further delayed.

Table 4 shows a comparison of the blast load scenarios at which initial yielding occurred and those at which fracture was first observed for each blast wall type. Yielding was observed the earliest in the stiffened blast wall and the latest in the corrugated blast wall with an intermediate section, which is consistent with the structural response analyzed in the previous paragraphs. Fracture was observed significantly later in the hybrid blast wall than in the other types, thus quantitatively demonstrating that the proposed design can effectively delay fracture initiation.

4. Conclusions

Blast walls, which are typically installed on offshore structures, were modeled using both analytical and numerical methods. Subsequently, blast load scenarios reflecting hydrogen explosion characteristics were selected, and the dynamic structural responses of the blast walls under these scenarios were investigated. The results are summarized as follows:

1. For all types of blast walls, under blast load scenarios with relatively low peak overpressures, elastic deformation was predominant and resonance significantly affected the dynamic structural response. Consequently, the maximum deformation occurred when the blast load duration was 0.5–1.0 times the natural period of the blast wall. However, as the peak overpressure of the blast loads increased, the stiffness degradation due to plastic deformation and the effect

of the blast load shape on the structural response became more pronounced, thus causing the maximum deformation to occur at longer blast load durations.

2. Despite being heavier than the corrugated blast wall, the stiffened blast wall exhibited greater displacements under the same blast load scenarios. Additionally, it reached the recommended deflection limits and ULS under scenarios with lower peak overpressures. This is attributed to its fixed-free boundary conditions and geometric features, which caused the buckling of the stiffener ends.
3. The von-Mises stress and plastic strain distributions showed that the area most susceptible to plastic deformation and fracture was the joints, including those between the panel and support, as well as those between the blast wall and deck, instead of the panels directly subjected to blast loads. This suggests that in blast-wall design, in particular when considering hydrogen blast loads that can cause substantial plastic deformation, the design of the connections is equally critical to that of the panels.

A hypothetical hybrid blast wall combining the advantages of both stiffened and corrugated blast walls was numerically modeled, and its dynamic structural response was investigated under hydrogen blast load scenarios. The hybrid blast wall exhibited enhanced stiffness as the peak overpressure increased, and fracture occurred at a higher peak overpressure compared with the case of the corrugated blast wall of the same mass. These results demonstrate its potential for application to blast wall design.

Acknowledgement

This work was supported by the National Research Foundation of Korea (NRF) grant funded by the Korea government (MSIT) (No. RS-2024-00348014).

Author Contributions

Conceptualization, H. -H. Lee and J. -K. Seo; Methodology, H. -H. Lee; Software, H. -H. Lee; Validation, H. -H. Lee and D. -K. Yang; Formal Analysis, H. -H. Lee and J. -K. Seo; Investigation, H. -H. Lee and J. -K. Seo; Resources, J. -K. Seo; Data Curation, H. -H. Lee and D. -K. Yang; Writing—Original Draft Preparation, H. -H. Lee; Writing—Review & Editing, H. -H. Lee and J. -K. Seo; Visualization, H. -H. Lee and D. -K. Yang; Supervision, J. -K. Seo; Project Administration, J. -K. Seo.

References

[1] H. D. Ng and J. H. S. Lee, “Comments on explosion problems for hydrogen safety,” Journal of Loss Prevention in the Process Industries, vol. 21, pp. 136-146, 2008.

[2] M. Kuznetsov, S. Kobelt, J. Grune and T. Jordan, “Flammability limits and laminar flame speed of hydrogen-air mixtures at sub-atmospheric pressures,” International Journal of Hydrogen Energy, vol. 37, pp. 17580-17588, 2012.

[3] R. Amirante, E. Distaso, P. Tamburrano, and R. D. Reitz, “Laminar flame speed correlations for methane, ethane, propane and their mixtures, and natural gas and gasoline for spark-ignition engine simulations,” International Journal of Engine Research, vol. 18, no. 9, pp. 951-970, 2017.

[4] Y. -H. Lee, M. -H. Cho, M. -C. Lee and Y. -J. Kim, “Evaluating hydrogen risk management policy PR: Lessons learned from three hydrogen accidents in South Korea,” International Journal of Hydrogen Energy, vol. 48, pp. 24536-24547, 2023.

[5] O. R. Hansen, “Hydrogen infrastructure-Efficient risk assessment and design optimization approach to ensure safe and practical solutions,” Process Safety and Environmental Protection, vol. 143, pp. 164-176, 2020.

[6] L. Mo, R. Wang, H. Yang, Y. Yang, X. Wu, W. Jia, C. Li and C. Chen, “Dynamic response of spherical tanks subjected to the explosion of hydrogen-blended natural gas,” Fuel, vol. 377, pp. 132834, 2024.

[7] J. Wang, Z. Liang, J. Lin, H. Feng, and S. Zhang, “Structural response for vented hydrogen-air deflagrations: Effects of volumetric blockage ratio,” Proceedings of the 4th International Symposium on Urban and Industrial Safety, pp. S284-S292, 2024.

[8] T. -T. Hao, C. -J. Wang, W. -J. Yan, W. -X. Ren, and K. -V. Yuen, “Experimental investigation on the dynamic responses of vented hydrogen explosion in a 40-foot container,” International Journal of Hydrogen Energy, vol. 46, pp. 19229-19243, 2021.

[9] Y. Du, F. Zhou, L. Zheng, W. Hu, B. Liao, L. Ma and J. Zheng, “Comparison of mode-I crack propagation of tube subjected to internal hydrogen static and detonation loading,” International Journal of Hydrogen Energy, vol. 45, pp. 11199-11210, 2020.

[10] P. Russo, A. D. Marco and F. Parisi, “Assessment of the damage from hydrogen pipeline explosions on people and buildings,” Energies, vol. 13, no. 19, pp. 5051, 2020.

[11] F. Liu, Z. Wang, X. Cao, P. Guo, Y. Lu, J. Xiao, and Y. Qian, “Experimental investigation on the dynamic reactions of concrete walls coated with blast-resistant materials to hydrogen explosions,” International Journal of Hydrogen Energy, vol. 142, pp. 490-497, 2025.

[12] Y. Du, Y. Liu, F. Zhou, Z. Li, L. Ma, and B. Liu, “Evaluation of blast wave from hydrogen pipeline burst by a coupled fluid-structure-rupture approach,” International Journal of Hydrogen Energy, vol. 55, pp. 696-703, 2024.

[13] D. Myilsamy, C. -B. Oh, and K. -S. Kim, “Numerical study on blast wall configurations on pressure behavior in high-pressure hydrogen tank explosions,” International Journal of Hydrogen Energy, vol. 93, pp. 1071-1087, 2024.

[14] G. -H. Go, V. -H. Cao, Y. -S. Kim, H. -J. Choi, S. -W. Oh and M. -J. Kim, “Evaluation of the dynamic stability of underground structures assuming a hydrogen gas explosion disaster in a shallow underground hydrogen storage facility,” Applied Sciences, vol. 13, no. 22, pp. 12317, 2023.

[15] S. Signetti, A. Klomfass, W. Riedel, R. Putzar, and A. Heine, “Simulation of blast propagation and structural effects of accidental hydrogen-air-mixture explosion in a two-stage light-gas gun laboratory for hypervelocity impact experiments,” Journal of Loss Prevention in the Process Industries, vol. 85, pp. 105138, 2023.

[16] X. Wang, B. Li, B. Han, X. Jin, D. Zhang, and M. Bi, “Explosion of high pressure hydrogen tank in fire: Mechanism, criterion, and consequence assessment,” Journal of Energy Storage, vol. 72, pp. 108455, 2023.

[17] M. Bratland, D. Bjerketvedt, K. Vaagsaether, “Structural response analysis of explosions in hydrogen-air mixtures in tunnel-like geometries,” Engineering Structures, vol. 231, pp. 111844, 2021.

[18] G. Atanga, S. Lakshmipathy, T. Skjold, H. Hisken, and A. G. Hanssen, “Structural response for vented hydrogen deflagrations: Coupling CFD and FE tools,” International Journal of Hydrogen Energy, vol. 44, pp. 8893-8903, 2019.

[19] J. E. Shepherd, “Structural response of piping to internal gas detonation,” Journal of Pressure Vessel Technology, vol. 131, no. 3, 2009.

[20] R. Krieg, B. Dolensky, B. Göller, W. Breitung, R. Redlinger and P. Royl, “Assessment of the load-carrying capacities of a spherical pressurized water reactor steel containment under a postulated hydrogen detonation,” Nuclear Technology, vol. 141, no. 2, pp. 109-121, 2003.

[21] B. -K. Jung, J. -H. Kim, and J. -K. Seo, “Investigation of the structural strength of existing blast walls in well-test areas on drillships,” Journal of Marine Science and Engineering, vol. 8, no. 8, 583, 2020.

[22] HSE, Analysis and Design of Profiled Blast Walls, Research Report 146, Health and Safety Executive, England, 2004.

[23] DNV, Design against Accidental Loads, DNV-RP-C204, Det Norske Veritas, Norway, 2010.

[24] J. M. Biggs, Introduce to Structural Dynamics, USA: McGraw-Hill, 1964.

[25] H. -H. Lee and J. -K. Seo, “Dynamic structural response of a corrugated blast wall under hydrogen blast loads,” Applied Sciences, vol. 15, no. 15, 8237, 2025.

[26] G. R. Cowper and P. S. Symonds, Strain Hardening and Strain Rate Effects in the Impact Loading of the Cantilever Beams, Technical Report TR-C11-28, Department of Applied Mathematics, University of Brown, USA, 1957.

[27] J. -M. Sohn, S. -J. Kim, J. -K. Seo, B. -J. Kim, and J. -K. Paik, “Strength assessment of stiffened blast walls in offshore installations under explosions,” Ships and Offshore Structures, vol. 11, no. 5, pp. 551-560, 2016.

[28] J. -M. Sohn, S. -J. Kim, B. -H. Kim, and J. -K. Paik, “Nonlinear structural consequence analysis of FPSO topside blast walls,” Ocean Engineering, vol. 60, pp. 149-162, 2013.

[29] LSTC, LS-DYNA Keywords User’s Manual: Volume I, California, USA: Livermore Software Technology Corporation, 2018.

[30] Standards Norway, “Actions and Action Effects,” Norway, N-003, 2007.

[31] FABIG, Design Guide for Stainless Steel Blast Walls, Technical Note 5, Fire And Blast Information Group, UK, 1999.

[32] S. Hassiotis and G. D. Jeong, “Identification of stiffness reductions using natural frequencies,” Journal of Engineering Mechanics, vol. 121, no. 10, pp. 1106-1113, 1995.

[33] A. Javanmardi, R. Abadi, A. K. Marsono, T. M. Tap, Z. Ibrahim, and A. Ahmad, “Correlation of stiffness and natural frequency of precast frame system,” Applied Mechanics and Materials, vol. 735, pp. 141-144, 2015.

[34] S. Timoshenko and S. Woinowsky-Krieger, Theory of Plates and Shells, McGraw-Hill, 1959.